Energy Engineering

Tech Science Press

DOI: 10.32604/EE.2021.016087

ARTICLE

Improved Thermophysical Properties of Developed Ternary Nitrate-Based Phase Change Material Incorporated with MXene as Novel Nanocomposites

I. Samylingam[1], Navid Aslfattahi[2], K. Kadirgama[1,*], Mahendran Samykano[3], L. Samylingam[4] and R. Saidur[4,5]

[1]Faculty of Mechanical & Automotive Engineering Technology, Universiti Malaysia Pahang, Pekan, Pahang, 26600, Malaysia

[2]Department of Mechanical Engineering, Faculty of Engineering, University of Malaya, Kuala Lumpur, 50603, Malaysia

[3]College of Engineering, Universiti Malaysia Pahang, Gambang, Pahang, 26300, Malaysia

[4]Research Centre for Nano-Materials and Energy Technology, School of Engineering and Technology, Sunway University, Petaling Jaya, 47500, Malaysia

[5]Department of Engineering, Lancaster University, Lancaster, LA1 4YW, UK

[*]Corresponding Author: K. Kadirgama. Email: kumaran@ump.edu.my

Received: 05 February 2021 Accepted: 10 June 2021

ABSTRACT

In this study, nanocomposite of ternary nitrate molten salt induced with MXene is developed. $LiNO_3$-$NaNO_3$-KNO_3 with wt% of 35:12:53 and 35:10:55 are produced and doped with MXene in the wt% of 0.2, 0.5, 1.0, and 1.5. FTIR result indicates the composites had no chemical reaction occurred during the preparation. UV-VIS analysis shows the absorption enhancement with respect to the concentration of MXene. Thermogravimetric analysis (TGA) was used to measure the thermal stability of the $LiNO_3$-$NaNO_3$-KNO_3 induced with MXene. The ternary molten salts were stable at temperature range of 600–700°C. Thermal stability increases with the addition of MXene. 1.5 wt% of MXene doped with $LiNO_3$-$NaNO_3$-KNO_3 with wt% 35:10:55 and 35:12:53, increases the thermal stability from 652.13°C to 731.49°C and from 679.82°C to 684.57°C, respectively. Using thermophysically enhanced molten salt will increase the efficiency of CSP.

KEYWORDS

Molten salt; MXene; TES; specific heat capacity; PCM

1 Introduction

After the release of poisonous gas into the atmosphere and death of fossil fuels, various green energy sources were identified. With the ongoing population growth and global development, uncertain volumes of resources are required. In pursuit of sustainable alternatives, solar energy has proved to be the highest producer of renewable sources. Sun provides us 120 000 TW energy per hour [1]. Photovoltaic (PV) and CSP are two well-known solar energy technologies. Sunlight in PV becomes a direct current through a semiconductor unit. The CSP facility consists of three major blocks: a solar receiver, liquid transmission system and a high-temperature control block. The sun ray focuses and coincides with the thermal field solar collection (HTF) and is then transferred into a thermal storage tank and transported to the production of electricity [2].

A major drawback in harvesting solar energy is, it is only available when there is sunlight. This can be overcome by using HTF as Thermal Energy Storage (TES). TES addresses the interval between the availability of solar power and the electricity needs, as well as reducing higher costs of electricity produced by CSP. Sensible TES was installed in industrial CSP plants in a two-tank molten salt facility. Latent TES with PCM is considered a cost- efficient option, since during transition process it provides higher energy storage density and insulating behaviour. It has been thoroughly studied in recent years and currently is transitioning from research by pilot-scale demonstration to commercial deployment [3–5].

Water is a good low-temperature sensible heat storage medium because it is inexpensive, has high specific heat and readily available. Its usage temperature is around 25–90°C. For 60°C temperature transition, waters store 250 kJ/kg. As transport medium and as energy storage, water, for instance, can be used for solar energy systems. However, it needs to be expensive isolation and stress tolerant because of its high vapour pressure for high temperature applications [6].

Because of the high temperature operating CSP systems, inorganic salts and salt eutectics with melting points above 300°C and metals and metal alloys are considered attractive candidates for PCMs [3,7,8]. In order to produce effective and stable PCM-TES systems the PCM should have the necessary high latent fusion heat, phase change temperature, reasonable chemical and thermal stability and reasonable corrosion in the containment material at high pressure and after repeated thermal [9–11].

Due to their massive latent melting heater, flexibility over a relative range of temperatures, an outstanding heat power and a huge variation of melting temperatures from one salt to another, the molten salts tend to be quite fascinating [12–14]. Salt mixtures with greater thermal stability can certainly provide better performance by extending the range of working temperatures [15,16]. Molten salts consisting of the sodium nitrate and potassium nitrate were used successfully in the big-scaled, SCR (Solar Control Power Panel) at temperatures up to 565°C [17] as a thermal energy collection and storage fluid. However, salt mixtures with lower melting points will increase performance by expanding the working temperature and by simplifying the start-up process [18,19]. The $NaNO_3$, KNO_3, and $NaNO_2$ ternary mixtures (7%–53%–40%) with the melting point of 142°C, will also typically be used in solar thermal power stations for heat transfer storage material. The molten salt is higher at the same pressure and the vapour pressure is below, the thermal conductivity doubles the volume of most organic thermal fluids. It also has the viscosity of high temperature water, making it an effective heat transfer and heat transfer storage material for thermal solar power [20]. Ternary molten salt is also environmental friendly and non-toxic [21]. Tab. 1 represents the recent studies on the ternary nitrate-based molten salts.

Table 1: Recent studies on ternary nitrate-based molten salts [22]

Compositions (wt%)	Melting point (°C)	Stability limit (°C)	Thermal conductivity (W/m K)
$NaNO_3$ (7)–KNO_3 (53)–$NaNO_2$ (40)	142	535	0.2
$NaNO_3$ (7)–KNO_3 (45)–$Ca(NO_3)_2$ (48)	120	500	0.52
$NaNO_3$ (28)–KNO_3 (52)–$LiNO_3$ (20)	130	600	N/A
Li_2CO_3 (32.1)–Na_2CO_3 (33.4)–K_2CO_3 (34.5)	400	800–850	N/A

However, its relative poor energy storage capacity is the biggest downside of molten salt acting as a heat carrier [23]. One of the main parameters influencing device size and output price is the basic heat capacity that specifically exposes the responsive heat that a material will store by unit mass or volume. Technical breakthroughs are important to enhance device performance and ultimately reduce the unit electricity price. Molten salt-based, special nature nanofluids will provide a potential alternative for reducing CSP

device sizes and costs. Shin et al. [24] observed that with the addition to carbonite eutectics of a limited number of nanoparticles of silica (not more than 1%) their particular heat potential could increase up to 24%. This rise was also detected by the dispersal of nanoparticles in various salts: CuO [25], Al_2O_3 [26] and TiO_2 [27].

The special physical and chemical properties of two dimensional (2D) materials have gained great interest after graphene was first rendered in a single layer in 2004 through mechanical exfoliation [28]. Recently, the latest class of 2D metal carbide/nitride intermediate materials known as MXene has received considerable attention from both theoretical and experimental physicists and chemists [29–32]. MXenes have excellent property such as high chemical stability, high electrical conductivity and eco-friendly characteristics due to their special structures. Up to now, the materials MXenes are promising in semi-conducting, hydrogen storage, supercapacitors, and lithium-ion batteries [33,34]. MXenes' hydrophilic nature and its large functions on its surface have rendered it successful in many molecular and ionic speed adsorbents MXenes.

In this research work, a novel nanocomposite with nitrate-based phase change materials is developed and induced with MXene to optimize the thermophysical properties. To the best of authors' knowledge, this is the first study of developing ternary nitrate-based nanocomposites incorporating promising MXene nanoparticles. This study has investigated various ratio of nitrate-based molten salts to develop two different types of ternary nitrate-based molten salts as host materials in order to develop novel nanocomposites. In this study, four samples are prepared with different concentrations of MXene nanoparticles.

2 Material and Method

Potassium nitrate is bought from Fisher Scientific chemicals with a molecular weight of 101.103 g/mol, the melting point of 337°C, the density of 2.1 g/m^3 and CAS-No 7757−79-1 Sodium nitrate ($NaNo_3$) is obtained from R&M chemicals Co with a molecular weight of 84.99 g/mol, melting point of 308°C, the density of 2.3 $g/m^{3,}$ and CAS-No 7631-99-4. Lithium nitrate ($LiNO_3$) with a molecular weight of 68.95 g/mol, melting point of 255°C, the density of 2.38 g/m^3 and CAS-No 7790-69-4 is purchased from Acros Organics chemical company. Fig. 1 shows the overall methodology flow chart.

2.1 Preparation of Ternary Molten Salt

$LiNO_3$-$NaNO_3$-KNO_3 salt was prepared at 35:12:53 wt%. 3.501 g of $LiNO_3$ was weighed using microbalance (TX323L, UNIBLOC) and added into 50 ml borosilicate beaker. 30 g of ultrapure deionized (DI) water was injected into the beaker. The mixture is stirred at 50°C on hotplate stirrer at 500 rpm for 30 min to dissolve $LiNO_3$ in DI water. In the beaker, 1.200 g $NaNO_3$ was added and stirred for further 30 min. 5.301 g KNO_3 has been added into beaker and stirred for another 1 h. Then the mixture is evaporated for 2 h at 140°C on hot plate. Finally, the salt is put in a dry oven at 140°C for 2 h to eliminate the chemically bonded water molecules. After 2 h, the samples were kept in a 20 ml disposable scintillation vial. The same process was repeated to produce $LiNO_3$-$NaNO_3$-KNO_3 salt with 35:10:55 wt%. Fig. 2 demonstrates the adopted methodology for the preparation of ternary nitrate-based molten salts.

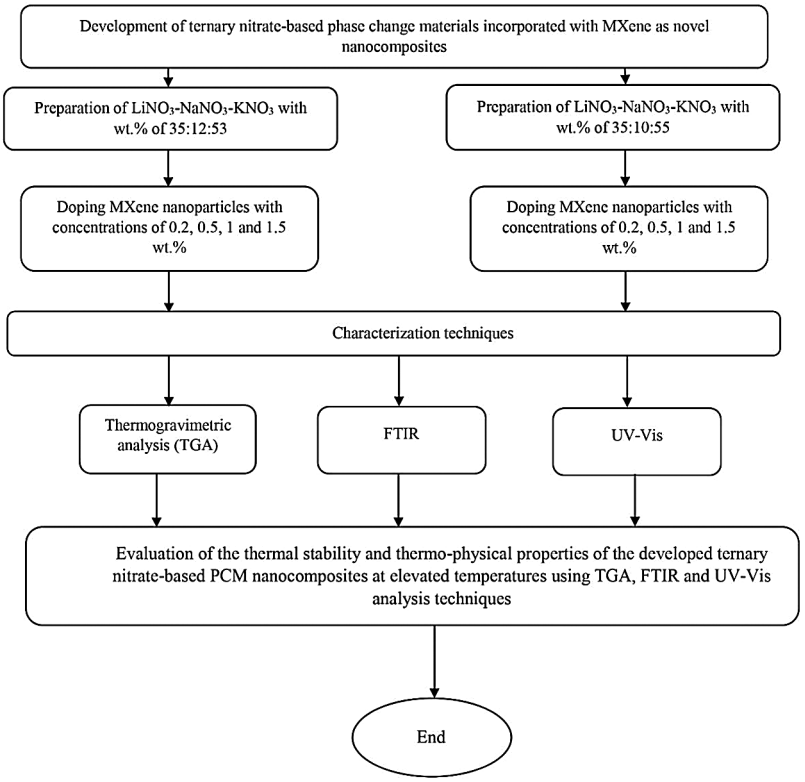

Figure 1: Overall methodology flow chart

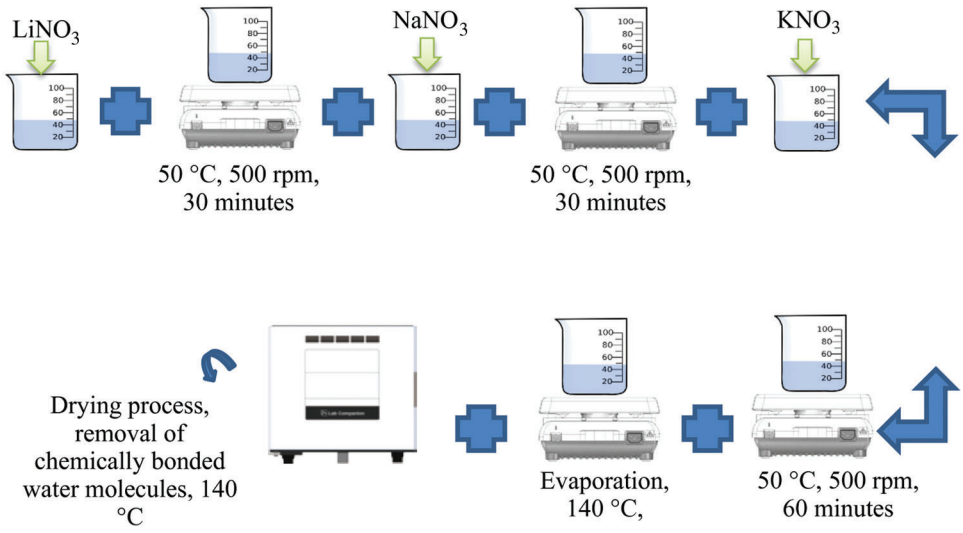

Figure 2: Preparation method of $LiNO_3$-$NaNO_3$-KNO_3 of (35:10:55) and $LiNO_3$-$NaNO_3$-KNO_3 (35:10:55)

2.2 Preparation of MXene ($Ti_3C_2T_x$)

MXene ($Ti_3C_2T_x$) synthesis process was conducted by the following materials as received without any further purification: MAX Phase material (Ti_3AlC_2) from Y-Carbon Inc., Ltd., USA, Ammonium hydrogen difluoride (reagent grade 95%, Sigma Aldrich) and sodium hydroxide (97% purity, pellets, Sigma Aldrich) were obtained. The wet-chemistry method was adopted for the synthesis of MXene nanomaterial. The

etching process was initiated by preparing a 2 M solution of NH_4HF_2 as the etchant for the synthesis process. The prepared 20 ml solution of ammonium hydrogen difluoride was placed on hot plate magnet stirrer (RCT BASIC, IKA), followed by stirring for one h at 300 rpm and room temperature. Afterward, 1 g of Ti_3AlC_2 was weighed using a microbalance (Explorer series, EX224, Ohaus), followed by adding to the uniform well-prepared NH_4HF_2 solution. Due to the exothermic reaction, the addition of MAX Phase (Ti_3AlC_2) to the NH_4HF_2 solution was performed slowly. In order to perform the etching process, the MAX Phase suspension in the NH_4HF_2 was stirred using magnetic stirrer at 300 rpm for 48 h and room temperature continuously. A dilute solution of NaOH was added slowly after completion of etching process until the pH of the settlement reached 6, and was filtered and rinsed several times with deionized water. The washing process took place in a high speed centrifuge (Sorvall LYNX 6000, Thermo Scientific) for 4 washes was performed (each wash of 10 min) at 3500 rpm. The obtained $Ti_3C_2T_x$ multi-layered solution was then sonicated using an ultrasonic probe sonicator (FS-1200 N) for 1 h to obtain delaminated MXene (d-$Ti_3C_2T_x$) in the setting of a power of 60% and on/off time of 7/3 s. By using vacuum oven (VO 500, MEMMERT Germany) the synthesized delaminated flakes of MXene nanomaterial were dried for overnight. The required characterizations for the synthesized MXene are available in our previous research study [19].

2.3 Preparation of $LiNO_3$-$NaNO_3$-KNO_3/MXene

Mixed with $LiNO_3$-$NaNO_3$-KNO_3 (35:12:53 wt%), are four distinct levels of MXene (0.2, 0.5, 1.0, and 1.5 wt%). Preparation of 0.2 wt% of MXene of $LiNO_3$-$NaNO_3$-KNO_3/MXene: 0,998 g molten salt was weighed in microbalance to a 100 ml of borosilicate beaker. The beaker added then 0.002 g MXene. The beaker holds 40 ml of DI water, with the mixture being extracted at 60°C and 700 rpm for 30 min. This is then accompanied by a 30 min stirring in ultrasonic probe sonicator (FS1200N) using 7-second duration on time and 3-second off time setting. Sonicator capacity is held at 55%. The mixture is then moved to a glass petri dish, placed on a hot plate for evaporation at temperature 120°C. After that, the petri dish is put in an oven (VO 500, MEMMERT GERMANY) with 60°C, 100 millibar of pressure for 1 h. The resulting nanocomposite is then placed in a vial (50 ml) until the thermophysical properties are calculated. This process is repeated to prepare 1 g each of $LiNO_3$-$NaNO_3$-KNO_3 (35:12:53 wt%)/MXene with the MXene concentration of 0.5, 1.0 and 1.5 wt% and $LiNO_3$-$NaNO_3$-KNO_3 (35:10:55 wt%)/MXene with the MXene concentration of 0.2, 0.5, 1.0 and 1.5 wt%. Fig. 3, illustrates the preparation method of ternary nitrate-based molten salts incorporated with MXene in various concentrations.

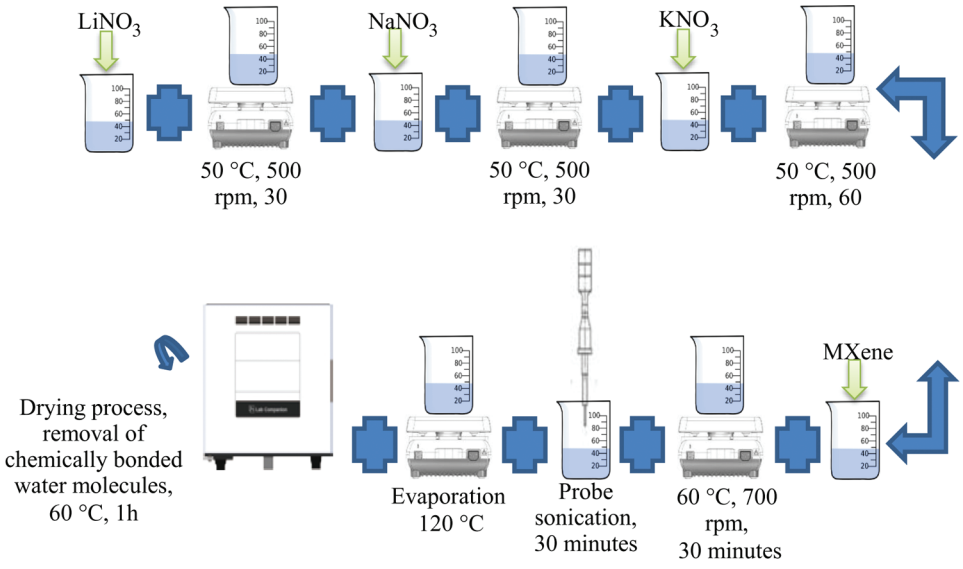

Figure 3: Preparation method of $LiNO_3$-$NaNO_3$-KNO_3/MXene with various concentrations

2.4 Characterisation

In this study, the specific heat capacity (c_p) and melting temperature measurements of the pure binary molten salt and alkali binary molten salt-based hBN nanocomposites are performed using a differential scanning calorimetry (DSC). DSC-8000 (Perkin Elmer, USA) is a double-furnace, power compensation DSC with greater sensitivity and accuracy instrument. The colorimetric and temperature accuracy of the above-mentioned DSC is considered as <±0.2% and ±0.05°C, respectively. The measurements are conducted using aluminum crucibles of 40 µl. The temperature range for measurements is between 25–500°C with the heating rate of 10°C/min. The c_p values and melting temperature analysis was through Pyris software.

2.4.1 FTIR

PerkinElmer Spectrum Two-UATR spectra with integrated detector of MIR TGS (15000-370 cm^{-1}) is used to detect the peak and the functional group of pure $LiNO_3$-$NaNO_3$-KNO_3 35:12:53 wt%, 35:10:55 wt%, $LiNO_3$-$NaNO_3$-KNO_3 (35:12:53 wt%)/MXene with the MXene concentration of 0.2, 0.5, 1.0, 1.5 wt%, and $LiNO_3$-$NaNO_3$-KNO_3 (35:10:55 wt%)/MXene with the MXene concentration of 0.2, 0.5, 1.0 and 1.5 wt%. The scanning speed used to detect the Fourier Transform Infrared Spectrum (FTIR) of the nanofluids is maintained constant 0.2 cm/s with the optimum scan range of 4000–450 cm^{-1}.

2.4.2 UV-Vis

PerkinElmer Lambda 750 is used to conduct Ultraviolet–visible spectroscopy (UV–Vis) to obtain optical absorbance. Absorption data is obtained at room temperature with the wavelength range from 800 to 200 nm. The scan speed adjusted is 266.75 nm/min with the 860 nm monochromatic.

2.4.3 Thermal Stability

Thermogravimetry analysis (TGA) of the $LiNO_3$-$NaNO_3$-KNO_3/MXene nanocomposites conducted using TGA 4000, Perkin Elmer. 5 mg of pure $LiNO_3$-$NaNO_3$-KNO_3 (35:12:53 wt%) was placed in 180 microlitre alumina crucible, which can withstand temperature up to 1750°C. The measurement was conducted under ultra-high pure nitrogen gas flow at 19.8 ml/min with 2.6 bar gas pressure. The temperature is raised from 30 to 900°C, with a heating rate of 10°C/min. The protocol was repeated with $LiNO_3$-$NaNO_3$-KNO_3 (35:12:53 wt%)/MXene with the MXene concentration of 0.2, 0.5, 1.0, 1.5 wt%, and $LiNO_3$-$NaNO_3$-KNO_3 (35:10:55 wt%)/MXene with the MXene concentration of 0.0 (pure), 0.2, 0.5, 1.0 and 1.5 wt% with the weight of 5 mg each. The data obtained is then analyzed using Pyris Software.

3 Results and Discussion

3.1 Thermogravimetric Analysis

The thermal stability of the molten salts is obtained using thermogravimetric analysis (TGA). Based on the outcome, the mixture of pure $LiNO_3$-$NaNO_3$-KNO_3 (35:10:55 wt%) salt has final residue temperature of 652.13°C. This value increases with the following rise in weight of the MXene doped: 668.97°C, 678.75°C, 696.45°C, 731.49°C for wt. percentage of 0.2%, 0.5%, 1.0% and 1.5%, respectively. The final residual temperature of pure $LiNO_3$-$NaNO_3$-KNO_3 with the wt% of 35:12:53 is 679.82°C. As the MXene percentage increases, the final residue temperature increases: 680.28°C, 664.80°C, 672.79°C, 684.57°C for wt% of 0.2, 0.5, 1.0 and 1.5, respectively. The experimentally obtained results are in accordance with the literature [5]. Figs. 4 and 5 shows the TGA graph plotted for tested samples. Tabs. 2 and 3 below show the result for pure ternary salt $LiNO_3$-$NaNO_3$-KNO_3 with 35:10:55 wt% and 35:12:53 wt% and MXene doped $LiNO_3$-$NaNO_3$-KNO_3 with 35:10:55 wt% and 35:12:53 wt%.

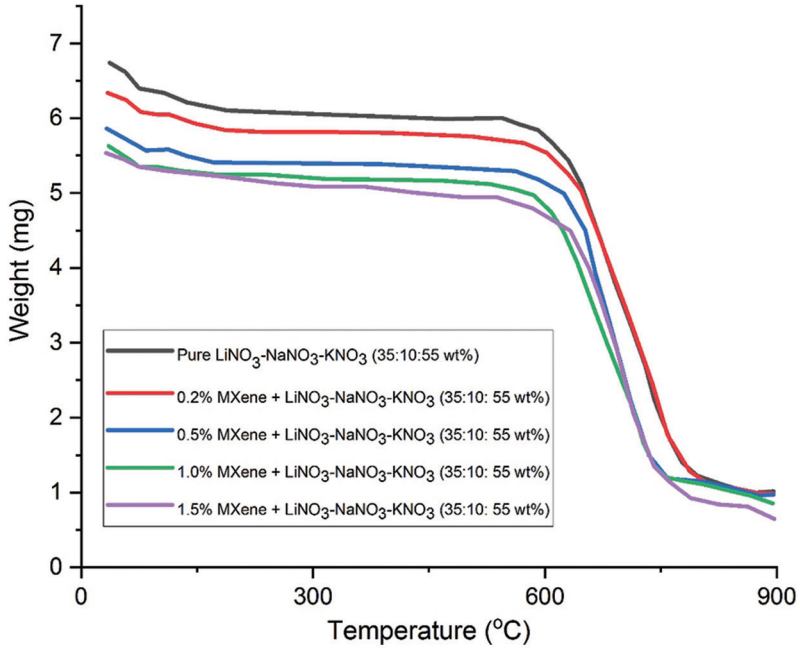

Figure 4: TGA curve for pure $LiNO_3$-$NaNO_3$-KNO_3 of (35:10:55) and $LiNO_3$-$NaNO_3$-KNO_3 (35:10:55) doped with MXene

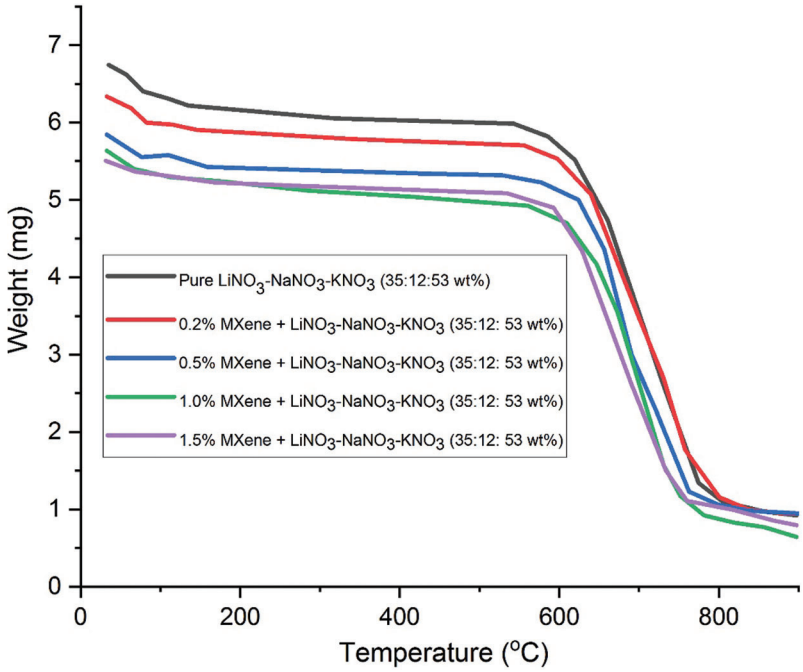

Figure 5: TGA curve for pure $LiNO_3$-$NaNO_3$-KNO_3 of (35:12:53) and $LiNO_3$-$NaNO_3$-KNO_3 (35:12:53) doped with MXene

Table 2: TGA result for pure $LiNO_3$-$NaNO_3$-KNO_3 of 35:10:55 wt% and MXene doped $LiNO_3$-$NaNO_3$-KNO_3 of 35:10:55 wt%

	Onset temperature (°C)	Final residue temperature (°C)
Pure $LiNO_3NANO_3KNO_3$ (35:10:55 wt%)	606.92	652.13
0.2% MXene + Pure $LiNO_3NANO_3KNO_3$ (35:10:55 wt%)	634.43	668.97
0.5% MXene + Pure $LiNO_3NANO_3KNO_3$ (35:10:55 wt%)	639.77	678.75
1.0% MXene + Pure $LiNO_3NANO_3KNO_3$ (35:10:55 wt%)	630.00	696.45
1.5% MXene + Pure $LiNO_3NANO_3KNO_3$ (35:10:55 wt%)	647.94	731.49

Table 3: TGA result for pure $LiNO_3$-$NaNO_3$-KNO_3 of (35:12:53) and MXene doped $LiNO_3$-$NaNO_3$-KNO_3 of (35:12:53)

	Onset temperature (°C)	Final residue temperature (°C)
Pure $LiNO_3NANO_3KNO_3$ (35:12:53 wt%)	631.63	679.82
0.2% MXene + Pure $LiNO_3NANO_3KNO_3$ (35:12:53 wt%)	629.66	680.28
0.5% MXene + Pure $LiNO_3NANO_3KNO_3$ (35:12:53 wt%)	619.38	664.80
1.0% MXene + Pure $LiNO_3NANO_3KNO_3$ (35:12:53 wt%)	640.40	672.79
1.5% MXene + Pure $LiNO_3NANO_3KNO_3$ (35:12:53 wt%)	644.43	684.57

3.2 FTIR Analysis

Figs. 6 and 7 show FTIR result for pure ternary salt $LiNO_3$-$NaNO_3$-KNO_3 with 35:10:55 wt% and 35:12:53 wt% and Mxene doped with $LiNO_3$-$NaNO_3$-KNO_3 35:10:55 wt% and 35:12:53 wt%. Peak at 3465 cm^{-1} shows stretching vibration of the OH groups. For ternary salt, the peaks at 1390 cm^{-1}, 1640 cm^{-1} and 1790 cm^{-1} were caused by the N-O stretching vibration and the peak at 836 cm^{-1} was caused by the N-O symmetric stretching vibration [35]. No other new peaks were found within the FT-IR spectrum of the composites. This result show that the composites were physical combined, no chemical reaction occurred during the preparation and the composites have good thermal stability [36,37].

3.3 UV-Vis Analysis

Figs. 8 and 9 shows UVVIS result for pure ternary salt $LiNO_3$-$NaNO_3$-KNO_3 with 35:10:55 wt% and 35:12:53 wt% and MXene doped with $LiNO_3$-$NaNO_3$-KNO_3 35:10:55 wt% and 35:12:53 wt%. As the concentration of MXene increases, the absorption increases. The stable position of absorbance peak indicates that new particles do not aggregate [38].

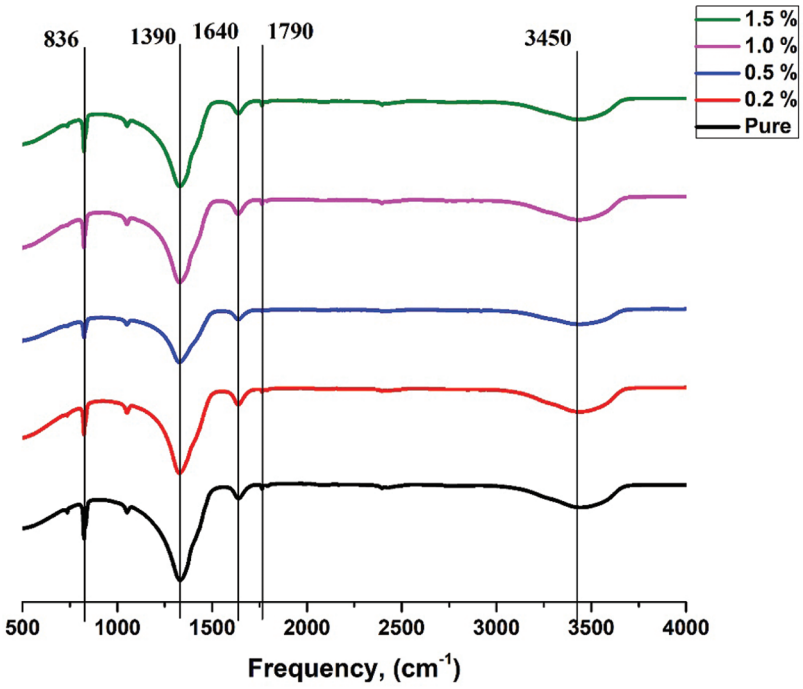

Figure 6: FTIR result for pure $LiNO_3$-$NaNO_3$-KNO_3 with 35:10:55 wt% and $LiNO_3$-$NaNO_3$-KNO_3 with 35:10:55 wt% doped with MXene

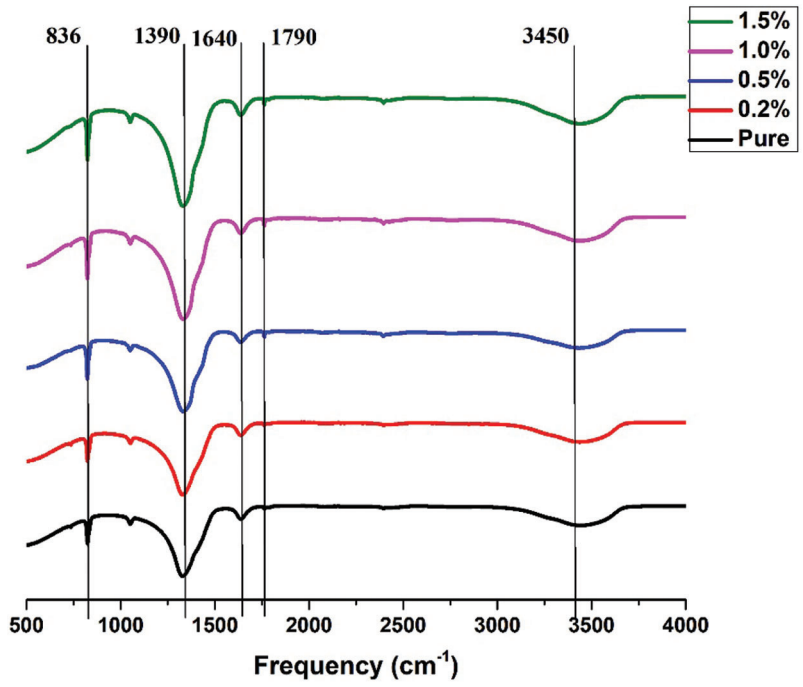

Figure 7: FTIR result for pure $LiNO_3$-$NaNO_3$-KNO_3 wit 35:12:53 wt% and $LiNO_3$-$NaNO_3$-KNO_3 with 35:12:53 wt% doped with MXene

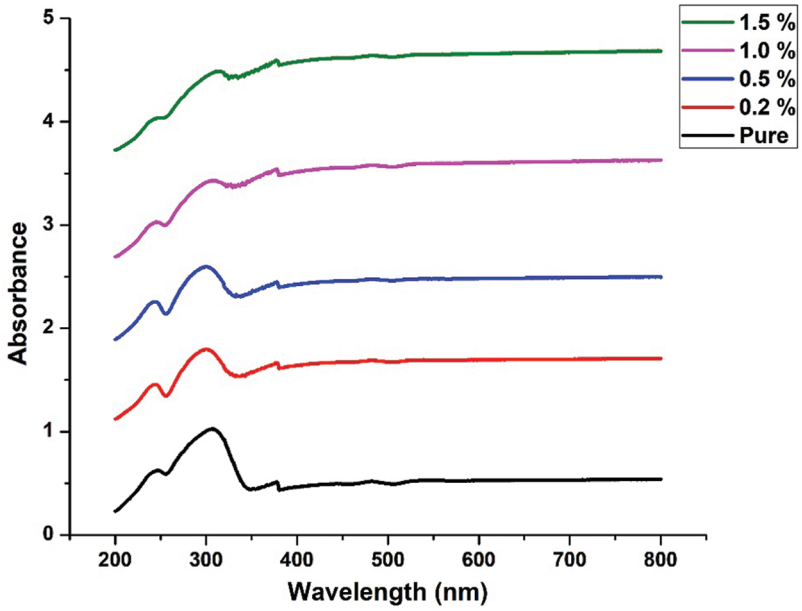

Figure 8: UV-VIS result for pure $LiNO_3$-$NaNO_3$-KNO_3 with 35:10:55 wt% and $LiNO_3$-$NaNO_3$-KNO_3 with 35:10:55 wt% doped with MXene

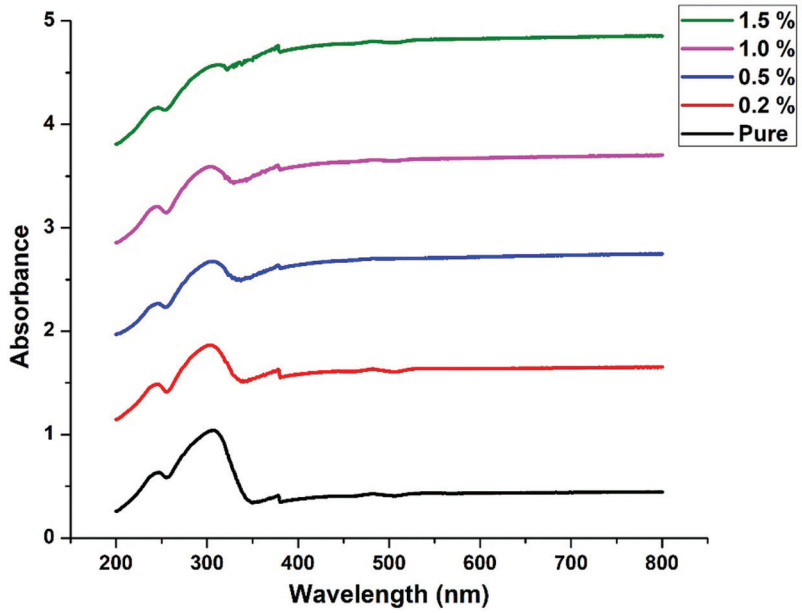

Figure 9: UV-VIS result for pure $LiNO_3$-$NaNO_3$-KNO_3 with 35:12:53 wt% and $LiNO_3$-$NaNO_3$-KNO_3 with 35:12:53 wt% doped with MXene

4 Conclusion

In this paper, thermal stability, FTIR and UVVIS analysis has been conducted on ternary nitrate salt of pure $LiNO_3$-$NaNO_3$-KNO_3 with the ratio of (35:10:55) and $LiNO_3$-$NaNO_3$-KNO_3 for the ratio of (35:12:53) are investigated by adding MXene as the nanoparticles with loading concentrations of 0.2, 0.5, 1.0, and 1.5 wt%. Thermal stability of the samples assessed using TGA. From the results obtained, ternary

eutectic salts are stable at temperatures between 600 and 700°C. With the addition of MXene the thermal stability increases. FTIR shows that composites were physical combined and no chemical reaction occurred during the preparation. UVVIS shows that the absorption increases with the concentration of MXene. Enhancing thermal stability would improve the thermal energy that can be retained before being injected to the power block for the production of electricity. This is critical as a higher temperature could be required to work in a turbine centered on the conventional Rankine cycle. Future studies could focus on the investigation of other important parameters, such as enthalpy, melting point, viscosity, specific heat and thermal conductivity.

Funding Statement: The authors are grateful to Minister of higher education under Fundamental Research Grant Scheme (FRGS) No. FRGS/1/2019/TK07/UMP/02/3 and Universiti Malaysia Pahang (www.ump.edu.my) for the financial support provided under the Grant, RDU192209.

Conflicts of Interest: The authors declare that they have no conflicts of interest to report regarding the present study.

References

1. Glaser, P. E. (1968). Power from the sun: Its future. *Science, 162(3856),* 857–861. DOI 10.1126/science.162.3856.857.
2. García, I. L., Álvarez, J. L., Blanco, D. (2011). Performance model for parabolic trough solar thermal power plants with thermal storage: Comparison to operating plant data. *Solar Energy, 85(10),* 2443–2460. DOI 10.1016/j.solener.2011.07.002.
3. Liu, M., Saman, W., Bruno, F. (2012). Review on storage materials and thermal performance enhancement techniques for high temperature phase change thermal storage systems. *Renewable and Sustainable Energy Reviews, 16(4),* 2118–2132. DOI 10.1016/j.rser.2012.01.020.
4. Aslfattahi, N., Samylingam, L., Abdelrazik, A., Arifutzzaman, A., Saidur, R. (2020). MXene based new class of silicone oil nanofluids for the performance improvement of concentrated photovoltaic thermal collector. *Solar Energy Materials and Solar Cells, 211,* 110526. DOI 10.1016/j.solmat.2020.110526.
5. Aslfattahi, N., Saidur, R., Sabri, M. F. M., Arifutzzaman, A. (2019). Experimental investigation on thermal stability and enthalpy of eutectic alkali metal solar salt dispersed with MgO nanoparticles. *The 4th International Tropical Renewable Energy Conference*, *10(6),* pp. 1112–1119. DOI 10.14716/ijtech.v10i6.3568.
6. Duffle, J. A., Beckman, W. A. (2013). *Solar engineering of thermal processes*. Wiley, New York. DOI 10.1002/9781118671603.
7. Kenisarin, M. M. (2010). High-temperature phase change materials for thermal energy storage. *Renewable and Sustainable Energy Reviews, 14(3),* 955–970. DOI 10.1016/j.rser.2009.11.011.
8. Aslfattahi, N., Saidur, R., Sidik, N. A. C., Sabri, M. F. M., Zahir, M. H. (2020). Experimental assessment of a novel eutectic binary molten salt-based hexagonal boron nitride nanocomposite as a promising PCM with enhanced specific heat capacity. *Journal of Advanced Research in Fluid Mechanics and Thermal Sciences, 68(1),* 73–85. DOI 10.37934/arfmts.68.1.7385.
9. Liu, M., Gomez, J., Turchi, C., Tay, N., Saman, W. et al. (2015). Determination of thermo-physical properties and stability testing of high-temperature phase-change materials for CSP applications. *Solar Energy Materials and Solar Cells, 139,* 81–87. DOI 10.1016/j.solmat.2015.03.014.
10. Zendehboudi, A., Aslfattahi, N., Rahman, S., Sabri, M. F. M., Said, S. M. et al. (2020). Optimization of thermal conductivity of NanoPCM-based graphene by response surface methodology. *Journal of Advanced Research in Fluid Mechanics and Thermal Sciences, 75(3),* 108–125. DOI 10.37934/arfmts.75.3.108125.
11. Krishna, Y., Aslfattahi, N., Saidur, R., Faizal, M., Ng, K. (2020). Fatty acid/metal ion composite as thermal energy storage materials. *SN Applied Sciences, 2(5),* 1–10. DOI 10.1007/s42452-020-2597-3.

12. Villada, C., Jaramillo, F., Castaño, J. G., Echeverría, F., Bolívar, F. (2019). Design and development of nitrate-nitrite based molten salts for concentrating solar power applications. *Solar Energy, 188,* 291–299. DOI 10.1016/j.solener.2019.06.010.
13. Zhang, P., Cheng, J., Jin, Y., An, X. (2018). Evaluation of thermal physical properties of molten nitrate salts with low melting temperature. *Solar Energy Materials and Solar Cells, 176,* 36–41. DOI 10.1016/j.solmat.2017.11.011.
14. D'Aguanno, B., Karthik, M., Grace, A., Floris, A. (2018). Thermostatic properties of nitrate molten salts and their solar and eutectic mixtures. *Scientific Reports, 8(1),* 1–15. DOI 10.1038/s41598-018-28641-1.
15. Baek, K., Jeon, W. C., Woo, S., Kim, J. C., Lee, J. G. et al. (2020). Synergistic effect of quinary molten salts and ruthenium catalyst for high-power-density lithium-carbon dioxide cell. *Nature Communications, 11(1),* 1–9. DOI 10.1038/s41467-019-14121-1.
16. Fernández, A. G., Muñoz-Sánchez, B., Nieto-Maestre, J., García-Romero, A. (2019). High temperature corrosion behavior on molten nitrate salt-based nanofluids for CSP plants. *Renewable Energy, 130,* 902–909. DOI 10.1016/j.renene.2018.07.018.
17. Herrmann, U., Kelly, B., Price, H. (2004). Two-tank molten salt storage for parabolic trough solar power plants. *Energy, 29(5–6),* 883–893. DOI 10.1016/S0360-5442(03)00193-2.
18. Herrmann, U., Kearney, D. W. (2002). Survey of thermal energy storage for parabolic trough power plants. *Journal of Solar Energy Engineering, 124(2),* 145–152. DOI 10.1115/1.1467601.
19. Aslfattahi, N., Saidur, R., Arifutzzaman, A., Sadri, R., Bimbo, N. et al. (2020). Experimental investigation of energy storage properties and thermal conductivity of a novel organic phase change material/MXene as a new class of nanocomposites. *Journal of Energy Storage, 27,* 101115. DOI 10.1016/j.est.2019.101115.
20. Nunes, V. M., Lourenço, M. J., Santos, F. J., Nieto de Castro, C. A. (2003). Importance of accurate data on viscosity and thermal conductivity in molten salts applications. *Journal of Chemical & Engineering Data, 48(3),* 446–450. DOI 10.1021/je020160l.
21. Coscia, K., Neti, S., Oztekin, A., Nelle, S., Mohapatra, S. et al. (2011). The thermophysical properties of the $NaNO_3$-KNO_3, $LiNO_3$-$NaNO_3$, and $LiNO_3$-KNO_3 systems. *ASME International Mechanical Engineering Congress and Exposition,* pp. 889–894. DOI 10.1115/IMECE2011-64465.
22. Vignarooban, K., Xu, X., Arvay, A., Hsu, K., Kannan, A. M. (2015). Heat transfer fluids for concentrating solar power systems–A review. *Applied Energy, 146,* 383–396. DOI 10.1016/j.apenergy.2015.01.125.
23. Andreu-Cabedo, P., Mondragon, R., Hernandez, L., Martinez-Cuenca, R., Cabedo, L. et al. (2014). Increment of specific heat capacity of solar salt with SiO_2 nanoparticles. *Nanoscale Research Letters, 9(1),* 582. DOI 10.1186/1556-276X-9-582.
24. Shin, D., Banerjee, D. (2011). Enhanced specific heat of silica nanofluid. *Journal of Heat Transfer, 133(2),* 501–505. DOI 10.1115/1.4002600.
25. Lasfargues, M., Stead, G., Amjad, M., Ding, Y., Wen, D. (2017). *In situ* production of copper oxide nanoparticles in a binary molten salt for concentrated solar power plant applications. *Materials, 10(5),* 537. DOI 10.3390/ma10050537.
26. Shin, D., Banerjee, D. (2014). Specific heat of nanofluids synthesized by dispersing alumina nanoparticles in alkali salt eutectic. *International Journal of Heat and Mass Transfer, 74,* 210–214. DOI 10.1016/j.ijheatmasstransfer.2014.02.066.
27. Lasfargues, M., Bell, A., Ding, Y. (2016). In situ production of titanium dioxide nanoparticles in molten salt phase for thermal energy storage and heat-transfer fluid applications. *Journal of Nanoparticle Research, 18(6),* 150. DOI 10.1007/s11051-016-3460-8.
28. Novoselov, K. S., Geim, A. K., Morozov, S. V., Jiang, D., Zhang, Y. et al. (2004). Electric field effect in atomically thin carbon films. *Science, 306(5696),* 666–669. DOI 10.1126/science.1102896.
29. Naguib, M., Kurtoglu, M., Presser, V., Lu, J., Niu, J. et al. (2011). Two-dimensional nanocrystals produced by exfoliation of Ti_3 AIC_2. *Advanced Materials, 23(37),* 4248–53. DOI 10.1002/adma.201102306.
30. Liu, J., Jiang, X., Zhang, R., Zhang, Y., Wu, L. et al. (2019). MXene-Enabled electrochemical microfluidic biosensor: Applications toward multicomponent continuous monitoring in whole blood. *Advanced Functional Materials, 29(6),* 1807326. DOI 10.1002/adfm.201807326.

31. Jiang, X., Kuklin, A. V., Baev, A., Ge, Y., Ågren, H. et al. (2020). Two-dimensional MXenes: From morphological to optical, electric, and magnetic properties and applications. *Physics Reports, 848,* 1–58. DOI 10.1016/j.physrep.2019.12.006.
32. Gao, L., Li, C., Huang, W., Mei, S., Lin, H. et al. (2020). MXene/polymer membranes: Synthesis, properties, and emerging applications. *Chemistry of Materials, 32(5),* 1703–1747. DOI 10.1021/acs.chemmater.9b04408.
33. Lee, Y., Cho, S. B., Chung, Y. C. (2014). Tunable indirect to direct band gap transition of monolayer Sc_2CO_2 by the strain effect. *ACS Applied Materials and Interfaces, 6(16),* 14724–14728. DOI 10.1021/am504233d.
34. Xing, C., Chen, S., Liang, X., Liu, Q., Qu, M. et al. (2018). Two-dimensional MXene (Ti_3C_2)-integrated cellulose hydrogels: Toward smart three-dimensional network nanoplatforms exhibiting light-induced swelling and bimodal photothermal/chemotherapy anticancer activity. *ACS Applied Materials & Interfaces, 10(33),* 27631–27643. DOI 10.1021/acsami.8b08314.
35. Lo, W. J., Shen, M. Y., Yu, C. H., Lee, Y. P. (1997). IR spectra and vibrational analysis of isotopomers of KNO_3 in solid Ar. *Journal of Molecular Spectroscopy, 183(1),* 119–128. DOI 10.1006/jmsp.1997.7265.
36. Guo, Q., Wang, T. (2015). Study on preparation and thermal properties of sodium nitrate/silica composite as shape-stabilized phase change material. *Thermochimica Acta, 613,* 66–70. DOI 10.1016/j.tca.2015.05.023.
37. Li, R., Zhu, J., Zhou, W., Cheng, X., Li, Y. (2016). Thermal compatibility of sodium nitrate/Expanded perlite composite phase change materials. *Applied Thermal Engineering, 103,* 452–458. DOI 10.1016/j.applthermaleng.2016.03.108.
38. Šileikaitė, A., Prosyčevas, I., Puišo, J., Juraitis, A., Guobienė, A. (2006). Analysis of silver nanoparticles produced by chemical reduction of silver salt solution. *Materials Science, 12(4),* 1392–1320. DOI 10.15282/ijame.10.2014.9.0160.